frontiers in Nanotechnology

ORIGINAL RESEARCH
published: 22 March 2021
doi: 10.3389/fnano.2021.659865

Coupling Hierarchical Ultrathin Co Nanosheets With N-Doped Carbon Plate as High-Efficiency Oxygen Evolution Electrocatalysts

Yue Wang[1], *Meng Li*[1], *Qixing Zhou*[2], *Qin Wang*[1], *Xingyuan Zhang*[1], *Dongmei Sun*[1]* *and Yawen Tang*[1]*

[1] *Jiangsu Key Laboratory of New Power Batteries, Jiangsu Collaborative Innovation Center of Biomedical Functional Materials, School of Chemistry and Materials Science, Nanjing Normal University, Nanjing, China,* [2] *School of Chemistry and Chemical Engineering, Southeast University, Nanjing, China*

OPEN ACCESS

Edited by:
Zexing Wu,
Qingdao University of Science and Technology, China

Reviewed by:
Wei Jin,
Chinese Academy of Sciences (CAS), China
Haitao Wang,
Wuhan Institute of Technology, China

***Correspondence:**
Dongmei Sun
sundongmei@njnu.edu.cn
Yawen Tang
tangyawen@njnu.edu.cn

Specialty section:
This article was submitted to Nanocatalysis, a section of the journal Frontiers in Nanotechnology

Received: *28 January 2021*
Accepted: *22 February 2021*
Published: *22 March 2021*

Citation:
Wang Y, Li M, Zhou Q, Wang Q, Zhang X, Sun D and Tang Y (2021) Coupling Hierarchical Ultrathin Co Nanosheets With N-Doped Carbon Plate as High-Efficiency Oxygen Evolution Electrocatalysts. Front. Nanotechnol. 3:659865. doi: 10.3389/fnano.2021.659865

The rational design of cost-effective and highly efficient catalysts for the oxygen evolution reaction (OER) is vastly desirable for advanced renewable energy conversion and storage systems. Tailoring the composition and architecture of electrocatalysts is a reliable approach for improving their catalytic performance. Herein, we developed hierarchical ultra-thin Co nanosheets coupled with N-doped carbon plate (Co-NS@NCP) as an efficient OER catalyst through a feasible and easily scalable NaCl template method. The rapid dissolution-recrystallization-carbonization synthesis process allows Co nanosheets to self-assemble into plenty of secondary building units and to distribute uniformly on N-doped carbon plate. Benefitting from the vertically aligned Co nanosheet arrays and hierarchical architecture, the obtained Co-NS@NCP possess an extremely high specific surface area up to 446.49 m^2 g^{-1}, which provides sufficient exposed active sites, excellent structure stability, and multidimensional mass transfer channels. Thus, the Co-NS@NCP affords remarkable electrocatalytic performance for OER in an alkaline medium with a low overpotential of only 278 mV at 10 mA cm^{-2}, a small Tafel slope, as well as robust electrocatalytic stability for long-term electrolysis operation. The present findings here emphasize a rational and promising perspective for designing high-efficiency non-precious electrocatalysts for the OER process and sustainable energy storage and conversion system.

Keywords: NaCl template, co nanosheets, N-doped carbon support, hierarchical structure, oxygen evolution reaction

INTRODUCTION

Urged by the ever-increasing consumption of fossil fuels and environmental pollution problems, numerous efforts have been put to design new renewable energy materials and technologies (Liu et al., 2020; Zhang X. et al., 2020; Zheng et al., 2020). Electrocatalytic oxygen evolution reaction (OER, $4OH^- \rightarrow 2H_2O + O_2 + 4e^-$) always draws significant attention in the scientific community because it plays a great crucial role in the development of energy conversion and storage technologies (e.g., metal-air batteries, water splitting devices) (Lyu et al., 2019; Yin et al., 2020).

However, the complex four-electron transfer process and high energy barriers of the formation of the O=O bond hinder the further applications of OER in energy-related applications (Xie et al., 2019; Jothi et al., 2020). Thus, it is necessary to develop high-efficiency electrocatalysts to expedite the reaction kinetics and reduce the overpotential for OER (Fu et al., 2018a; Wang and Zeng, 2018; Chen R. et al., 2019). Up till now, noble-metal-based oxides, such as IrO_2 and RuO_2, are commonly acknowledged as state-of-the-art electrocatalysts for the OER. But the scarcity reserves and high prices of these noble metals greatly limit the realization of large-scale commercialization (Fu et al., 2018b; Sun et al., 2020b). Therefore, the exploration of both economical and efficient non-noble-metal-based OER electrocatalysts to replace these noble metals has become a research trend (Fu et al., 2018c; Wu et al., 2020).

In recent years, as a potential substitute for commercial IrO_2 and RuO_2 catalysts, noble-metal-free-based catalysts have been widely researched. Among them, earth-abundant Co-based electrocatalysts, including oxides (Li T. et al., 2019; Zhang Y. et al., 2020), sulfides (Dong et al., 2019; Fragal et al., 2019), phosphides (Jin et al., 2019; Li M. et al., 2020), nitrides (Ouyang et al., 2019; Yang et al., 2019b), layered double hydroxides (LDHs) (Yu et al., 2017; Dionigi et al., 2020), metal-organic frameworks (MOFs) (Chen et al., 2017; Kang et al., 2019), single atoms (Yang et al., 2018; Zang et al., 2018), etc., have been proven to have a low price and good electrocatalytic activity toward OER process (Yang et al., 2019a; Zhao et al., 2020; Zhu et al., 2020). In particular, Co species supported on carbonaceous materials, such as nitrogen-doped carbon nanotubes (NCNTs) (Zhao et al., 2018; Huang et al., 2020), reduced graphene oxide (rGO) (Li Y. et al., 2018), and porous carbon (Fu et al., 2018d) electrocatalysts have demonstrated greatly enhanced electrocatalytic activity and stability. For example, Jiao et al. designed and developed a molecule-level graphitic carbon nitride (g-C_3N_4) coordinated transition metal Co catalyst (Co-C_3N_4/CNT), which possessed comparable electrocatalytic activity to that of the noble metal catalysts for the ORR and OER in alkaline solution (Zheng et al., 2017). The intimate connections between active Co and g-C_3N_4 could inhibit the aggregation and dissolution of active sites during the catalytic process. In addition, structural engineering is one of the outstanding approaches to improve the catalytic activity and reaction rate of OER (Li S. et al., 2019; Chandrasekaran et al., 2020). The construction of special nanostructures (e.g., hollow structure, hierarchical structure, nanoarray architectures, etc.) can endow the electrocatalysts with a higher specific surface area to expose more active sites and possess more mass transport channels to enhance the rate of reaction (Fu et al., 2017a; Cheng et al., 2019; Wang S. et al., 2019; Zhang, C.-L. et al., 2020). For instance, Guan et al. designed and synthesized a three-dimensional (3D) hierarchical CoNi/$CoFe_2O_4$ supported on Ni foam, which delivered a cell voltage of only 1.57 V at a current density of 10 mA cm^{-2} for overall water splitting (Li S. et al., 2018). For self-assembled hierarchical structure, the *in situ* formed self-supported hierarchical structure could provide numerous more accessible active sites (Sun et al., 2020a). Besides, the self-supported structure and the presence of substrate will prevent the aggregation and stratification of active substances, facilitate the permeation of electrolyte, enlarge the specific surface area and release bubbles to accelerate the reaction kinetics (Li T. et al., 2020). The construction of a hierarchical structure on carbon supports will also provide an intimate contact interface between the active substance and the supports, which will facilitate and improve the electrical conductivity (Zhou et al., 2020). Taken together, the design and construction of self-supported hierarchically Co-based catalysts on carbon substrate should be able to deliver a satisfactory catalytic performance with improved catalytic activity and robust stability (Yang et al., 2019c).

Herein, we reported a novel and efficient catalyst composed of hierarchically ultra-thin Co nanosheets arrays coupled with N-doped carbon plate (denoted as Co-NS@NCP) for a highly-efficient OER process. Through the rapid dissolution-recrystallization-carbonization synthesis process, the self-assembled Co nanosheet arrays and 2D carbon plates are well-formed on the stable 2D platform surface of NaCl hard-template. The hierarchical and porous structure of the Co-NS@NCP provides a high specific surface area (446.49 cm^2 g^{-1}), abundant exposed active sites, excellent structure stability, and multidimensional mass transfer channels. Thus, the resulting Co-NS@NCP catalyst displays an excellent OER performance with a low overpotential at 10 mA cm^{-2} (only 278 mV), a small Tafel slope, as well as steady electrocatalytic stability, which significantly superior to that of commercial RuO_2.

RESULTS AND DISCUSSION

The fabrication process of the Co-NS@NCP catalyst is schematically described in **Figure 1**. The Co^{2+}- histidine@NaCl complexes were first synthesized by the rapid dissolution and recrystallization of $Co(NO_3)_2{\cdot}6H_2O$, histidine, and excessive NaCl precursors. Histidine, as one of the essential amino acids, not only has good coordination ability with metal ions, which is essential for the formation of M-N-C (e.g., Co^{2+}, Ni^{2+}, Fe^{3+}) (Chen Y. et al., 2019) (**Supplementary Figure 1**) but also plays a role of cheap, green and non-toxic sources of N and C. Besides, excessive NaCl was chosen as a hard-template which provides a stable 2D platform for the formation and growth of Co nanosheets and carbon plate (Fu et al., 2017b; Huan et al., 2019). By rapid dissolution and recrystallization process, histidine and Co precursors were uniformly deposited on the surface of NaCl nanocrystals, as observed from the SEM images in **Figure 1**. After pyrolysis at 700°C for 2 h under N_2 atmosphere, the Co^{2+}-histidine@NaCl complexes were converted into ultrathin Co nanosheets coupled with N-doped carbon plate (Co-NS@NCP) loaded on NaCl nanocube. During the annealing process, histidine was transformed into N-doped carbon plate and Co species were reduced to Co nanosheets on the surface of the N-doped carbon plate. Finally, after removing the inside NaCl template with water/ethanol and centrifugation, the 2D ultrathin Co-NS@NCP was obtained. For comparison, Co-NS@NCP-600, Co-NS@NCP-650, and Co-NS@NCP-750 samples were prepared *via* a similar process except with different pyrolysis temperatures at 600, 650, and 750°C, respectively. The

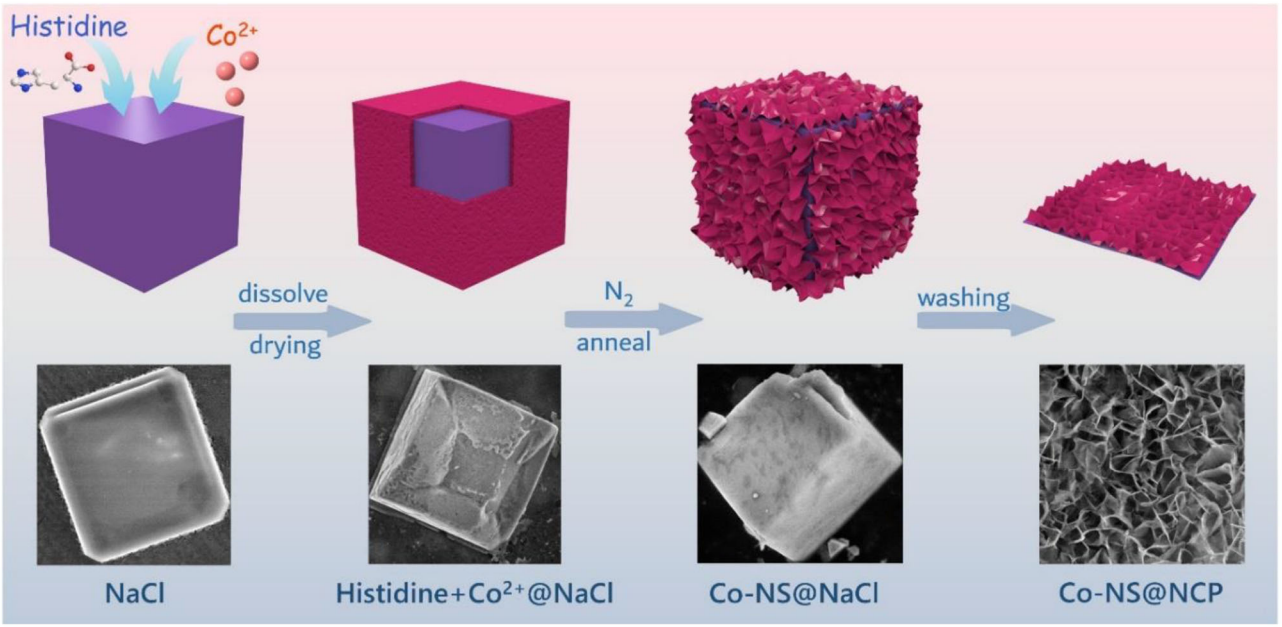

FIGURE 1 | Schematic illustration and SEM images of the formation process of Co-NS@NCP catalyst.

detailed experiment process was described in the Experimental section. The composition and crystal structure of Co-NS@NCP was also verified by the corresponding X-ray diffraction (XRD) pattern. As shown in **Supplementary Figure 2**, a set of diffraction peaks located at 44.2, 51.5, and 75.8° can be well indexed to (111), (200), and (220) facets of metallic Co phase (JCPDS Card No. 15-0806) while a broad diffraction peak at about 26° is corresponding to (002) plane of graphitic carbon.

The morphology and structure features of Co-NS@NCP were first investigated by scanning and transmission electron microscopy (SEM and TEM) images. As revealed by **Figures 2a,b**, the as-fabricated Co-NS@NCP catalyst presents a porous hierarchical structure consisted of ultrathin 2D sheet-like Co nanoarrays which are uniformly distributed on the surface of the carbon plate. XRD patterns and SEM images of Co-NS@NCP at different pyrolysis temperatures (**Supplementary Figures 3–5**) demonstrate that the composition of the products did not change significantly while the density of Co nanosheets array structures enhanced with the increase of pyrolysis temperature. When the pyrolysis temperature goes up to 750°C, the array structures of Co-NS@NCP collapsed. Therefore, 700°C is the optimal pyrolysis temperature for the synthesis of Co-NS@NCP catalysts. Due to the highly open hierarchical architecture and porosity features, the Co-NS@NCP catalyst possesses a high Brunauer-Emmett-Teller (BET) surface area up to 446.49 $m^2 g^{-1}$. The pore-size distribution curve (**Supplementary Figure 6**) shows the presence of micropores and mesopores in the Co-NS@NCP-700 catalyst. N_2 adsorption-desorption isotherms (**Figure 2c**) depict typical IV-type characteristics, indicating the typical mesoporous features of Co-NS@NCP, which in accordance well with the SEM and TEM images. The high specific surface area and highly open hierarchical architecture of Co-NS@NCP could provide more accessible active-sites and a large number of electron/mass transfer pathways during the electrocatalysis process (Chen J. et al., 2019). Magnified SEM and TEM images (**Figures 2d,e**) reveal that the flexible and ultrathin Co nanosheets were interconnected and self-assembled into many secondary building-units. The thickness of the Co nanosheet was measured about 4 nm, as obtained from the magnified SEM image. The high-resolution TEM (HRTEM) image (**Figure 2f**) depicts the well-resolved interplanar lattice spacing of 0.21 nm, corresponding to the (111) plane of cubic Co phase, which in accordance well with the XRD results above. Notably, lattice dislocations and defects can also be observed in the HRTEM image, which may be caused by the curling and interlacing of flexible nanosheets. The atoms at lattice dislocations and defects could facilitate the catalytic process effectively by working as catalytic active sites due to their coordinative unsaturation nature (Zhou et al., 2019). Scanning TEM (STEM) image (**Figure 2g**), corresponding energy-dispersive X-ray (EDX) element mapping images (**Figure 2h**), and line scanning profiles (**Supplementary Figure 7**) indicating the uniform interspersion of Co, N and C in the Co-NS@NCP catalyst. The mass ratio of Co, C, and N elements was measured to be 60.57: 33.27: 6.15 embodied by the EDX spectrum (**Figure 2i**). Thermogravimetry analysis (TGA) was conducted to further appraise the proportion of Co element in Co-NS@NCP. As demonstrated in **Supplementary Figure 8**, the TGA curve has a significant weight loss at 300–400°C, which is mainly due to the weight loss of caron nanosheets and the oxidation of

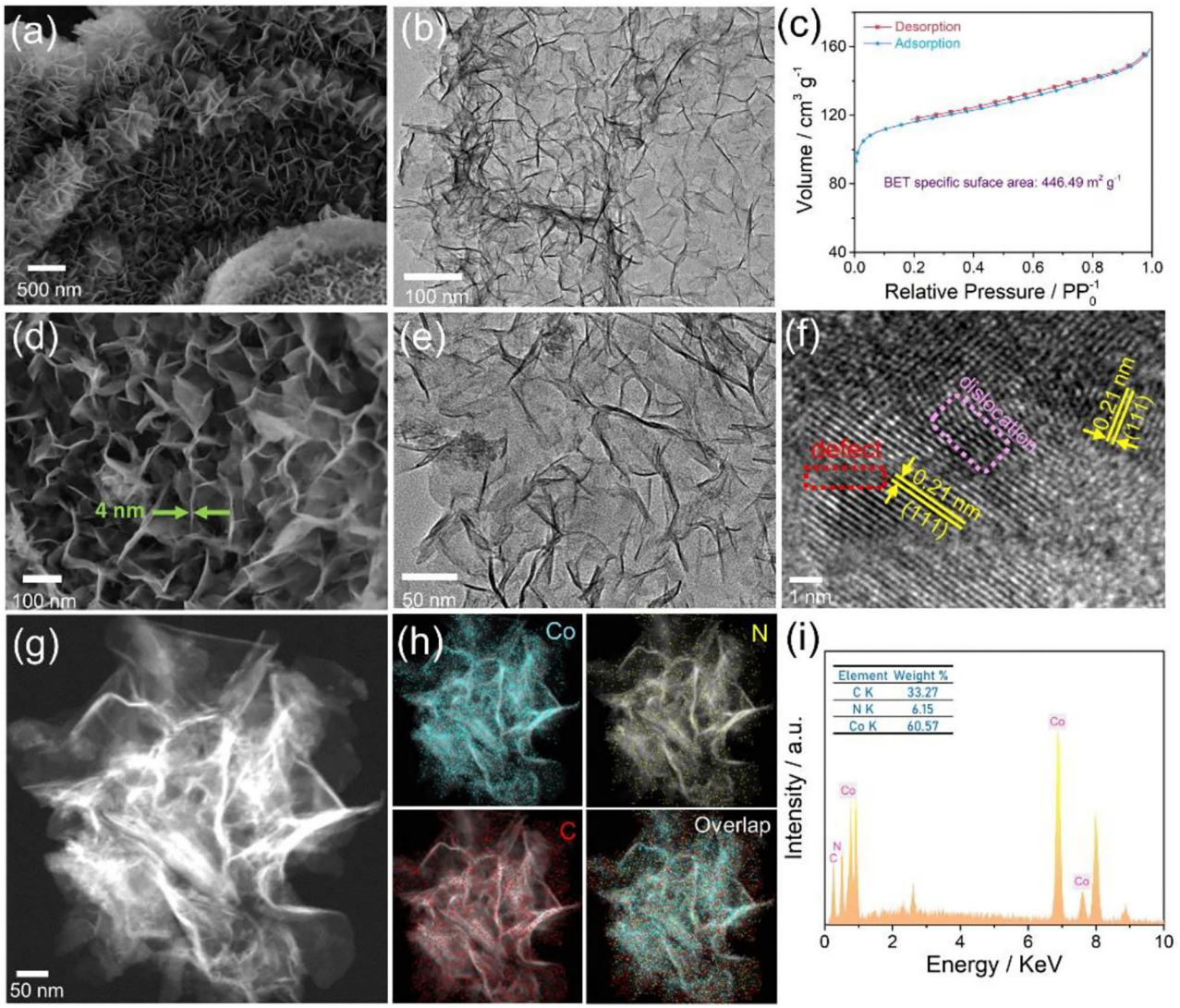

FIGURE 2 | Morphology characterization of the composite Co-NS@NCP: Large-area **(a)** SEM and **(b)** TEM images; **(c)** N_2 adsorption-desorption isotherms; **(d)** Magnified SEM and **(e)** TEM images; **(f)** HRTEM image; **(g)** HAADF-STEM image and **(h)** corresponding EDX element mapping images; **(i)** EDX spectrum.

the Co element. The weight content of the Co element in the Co-NS@NCP was estimated to be about 59.97 wt.% in light of the residual weight of Co_3O_4.

X-ray photoelectron spectroscopy (XPS) was further conducted to examine the composition and surface chemical valance states of Co-NS@NCP catalyst. The XPS survey scan spectrum in **Supplementary Figure 9** confirms the co-existence of Co, C, and N elements in the resulting Co-NS@NCP catalyst, in accordance well with EDX results. The high-resolution Co 2p XPS spectrum in **Figure 3A** shows two main typical peaks at 780.3 and 795.6 eV, indicating the presence of $2p_{3/2}$ and $2p_{1/2}$ orbits of Co^{3+} and Co^{2+} species, respectively; while the peaks at 787.5 and 803.5 eV could be attributed to associated shake-up satellites. The existence of oxidate Co species could be ascribed to the surface oxidation of the Co-NS@NCP catalyst when exposing to air. The high-resolution C 1s spectrum (**Figure 3B**) proves an obvious sp^2-hybridized C-C peak at 284.6 ev (Wang et al., 2020). It was notable that the peak ascribed to the C-N bond could be clearly observed at 285.4 eV, indicating the successful doping of the N element in the carbon plate. The N 1s spectrum (**Figure 3C**) can be well-assigned to three bonding types of N species, pyridinic N (398.1 eV), pyrrolic N (400.4 eV), and graphitic N (401.9 eV), respectively (Wang H. et al., 2019). Raman spectroscopy was executed to further explore the structural characteristic of the Co-NS@NCP catalyst. As shown in **Figure 3D**, there are two typical peaks located at about 1350 and 1580 cm^{-1} for all the Co-NS@NCP catalysts, according to the D-band (disordered carbon atoms) and G-band (graphitic carbon atoms), respectively (Fragal et al., 2019). All of the Co-NS@NCP samples at different temperatures exhibit

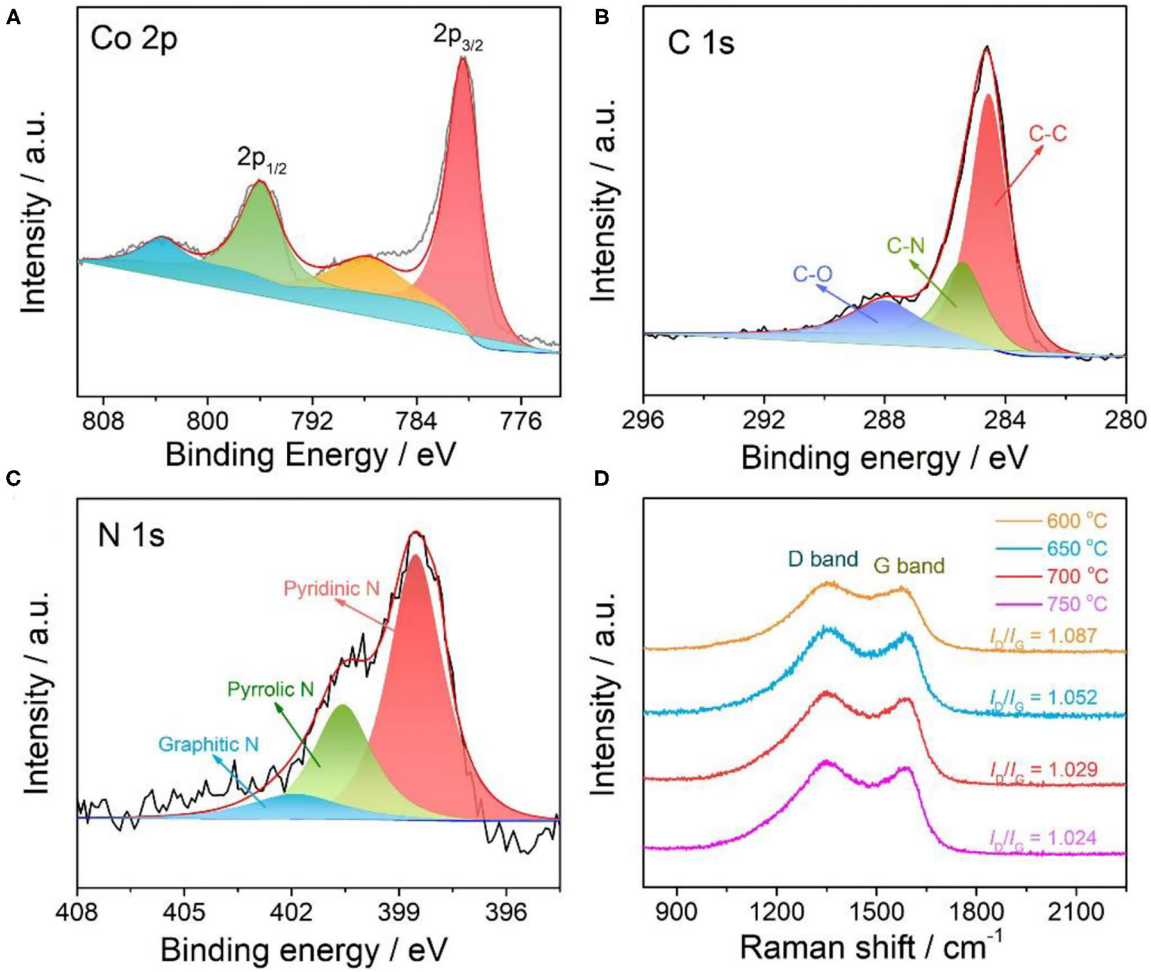

FIGURE 3 | High-resolution XPS spectra of **(A)** Co 2p region, **(B)** C 1s region, and **(C)** N 1s region, respectively; **(D)** Raman spectrum of Co-NS@NCP.

a high-intensity ratio of D-band and G-band (I_D/I_G), which suggests the high number of defects that origin from the size and bonding state difference between C and N atoms in the N-doped carbon. The high content of nitrogen species and high structural defects in Co-NS@NCP catalyst could result in faster charge transfer rates and induce more catalytically active sites toward the catalytic process (Yu et al., 2018).

The electrocatalytic performance of the as-fabricated Co-NS@NCP catalyst for OER was investigated in an O_2-saturated 1.0 M KOH solution with a standard three-electrode system. For comparison, the catalytic performance of commercial RuO_2 and Co-NS@NCP catalysts obtained at different annealing temperatures were also recorded under identical conditions. All potentials in the polarization curves have not been iR-corrected. **Figure 4A** depicted the linear sweep voltammetry (LSV) polarization curves of Co-NS@NCP catalysts obtained at different annealing temperatures. The Co-NS@NCP sample at pyrolysis temperature of 700°C reveals the best OER electrocatalytic activities. Co-NS@NCP-700 exhibits the highest current density during the overall LSV polarization curves. The activity decreased regardless of the pyrolysis temperature increases or decreases, which could be ascribed to the structure superiority of Co-NS@NCP-700. According to **Figure 4A**, the overpotentials at the current density of 10 mA cm^{-2} of all the samples were summarized in **Figure 4B**. The Co-NS@NCP-700 sample delivers a low overpotential of only 278 mV at the current density of 10 mA cm^{-2}, which is significantly lower than that of Co-NS@NCP-600 (396 mV), Co-NS@NCP-650 (391 mV), and Co-NS@NCP-750 (383 mV). The low overpotential of Co-NS@NCP-700 is even superior to the commercial RuO_2 (342 mV) and lower than most of the previously reported Co-based electrocatalysts (**Supplementary Table 1**). The OER kinetics and mechanism of all the samples were investigated by Tafel plot which calculated from the polarization curves (Chen et al., 2020). As depicted in **Figure 4C**, the Co-NS@NCP-700 sample exhibits a favorable Tafel slope value of 95.9 mV cm^{-2} which is competitive to commercial RuO_2 (101.6 mV cm^{-2}) and clearly less than Co-NS@NCP-600 (126.4 mV cm^{-2}), Co-NS@NCP-650 (135.6 mV cm^{-2}), and Co-NS@NCP-750 (125.1 mV cm^{-2}). The low Tafel slope of Co-NS@NCP-700 manifests that the Co-NS@NCP-700

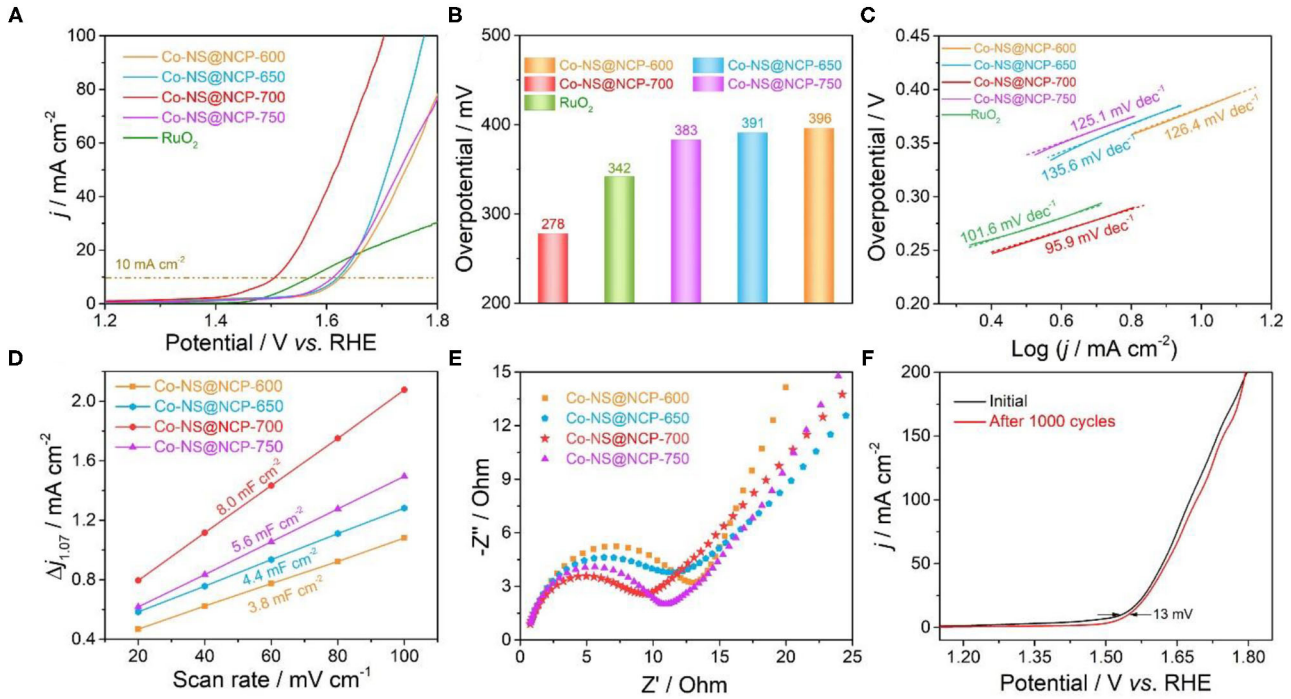

FIGURE 4 | Electrocatalytic OER performance of different samples in 1.0 M KOH electrolyte: **(A)** LSV polarization curves; **(B)** overpotentials at a current density of 10 mA cm^{-2}; **(C)** Tafel plots derived from the panel; **(D)** C_{dl} values; **(E)** EIS Nyquist plots; **(F)** LSV polarization curves of the Co-NS@NCP-700 catalyst before and after 1,000 cycles.

employs the first discharge step (i.e., the chemical adsorption of OH^- species: $M + OH^- \rightarrow$ M-OH + e^-) as a rate-limiting step and influences the reaction kinetics (Xu et al., 2019).

To estimate the authentic catalytic active site number of Co-NS@NCP for the OER process, the electrochemical double-layer capacitance (C_{dl}) of all the Co-NS@NCP samples were assessed by a cyclic voltammetry curve (CV) with different scan rates at non-Faradaic potential region (**Supplementary Figure 10**). Normally, the C_{dl} values are positively linearly proportional to the electrochemical surface area (ECSA) at the solid-liquid interface (Xu et al., 2020). As shown in **Figure 4D**, the Co-NS@NCP-700 catalyst exhibits a C_{dl} value of 8.0 mF cm^{-2}, which larger than that of other samples of different temperatures (Co-NS@NCP-600: 3.8 mF cm^{-2}, Co-NS@NCP-650: 4.4 mF cm^{-2}, and Co-NS@NCP-750: 5.6 mF cm^{-2},). Besides, the electrochemical impedance spectroscopy (EIS) measurement was further executed to estimate the reaction kinetics during the OER process (Zhu et al., 2019). As shown in Nyquist plots measured at 1.57 V (**Figure 4E**), the Co-NS@NCP-700 catalyst displays the smallest charge transfer resistance (R_{ct}) in all catalysts obtained at different pyrolysis temperatures, demonstrating a good charge transfer resistance and faster OER kinetics. The stability of the Co-NS@NCP-700 sample is also examined by running sequential 1,000 CV scanning cycles. As depicted in **Figure 4F**, the LSV curve of Co-NS@NCP-700 after 1,000 CV cycles is almost the same as the previous one. The overpotential of OER at the current density of 10 mA cm^{-2} only increased by 13 mV, demonstrating excellent electrochemical stability in an alkaline medium. Long-term *i–t* chronoamperometric teat was also executed to verify the good electrochemical stability of Co-NS@NCP-700. In O_2-saturated 1.0 M KOH solution, the current density of Co-NS@NCP-700 remains stable under sequential *i-t* test at a constant potential of 1.51 V for even over 12 h (**Supplementary Figure 11a**). XPS characterization of Co-NS@NCP-700 sample before and after the *i-t* test (**Supplementary Figure 11b**) indicates that the peaks of high-resolution Co 2p spectrum of Co-NS@NCP-700 shift to higher binding energies after *i-t* test, which may be attributed to the surface oxidation of Co-NS@NCP-700 catalyst at high oxidation potential during OER process. To evaluate the quantity of catalyst comprehensively, the Faradic efficiency of Co-NS@NCP-700 during the OER process was also measured through the drainage gas collector device (**Supplementary Figure 12a**). As depicted in **Supplementary Figure 12b**, the experimental and theoretical O_2 yield-time curve is almost overlapped at a constant current density of 20 mA cm^{-2}. Thus, the calculated Faradic efficiency is nearly 100%, indicating the ultrahigh selectivity of the Co-NS@NCP-700 catalyst for OER. Taken together, the outstanding OER activity, stability, and selectivity of Co-NS@NCP makes it a promising non-precious metal catalyst for OER with low cost and high efficiency.

The excellent OER performance is greatly associated with the vertically aligned ultrathin Co nanosheet arrays and hierarchically porous architecture of Co-NS@NCP catalyst (Zhou

et al., 2017). First, the self-supported and vertically aligned ultrathin Co nanosheet arrays possess a large number of more accessible active sites, which is favorable to facilitate the OER process (Hua et al., 2019; Zhang et al., 2019). Second, the hierarchically porous architecture of Co-NS@NCP has prominent structural advantages that not only provide a highway for mass diffusion/transport but also prohibit the mutual stacking and aggregation of nanosheets during the OER process (Mishra et al., 2018). Last but not least, the N-doped carbon plate, which serves as a good electron conductor, could boost the interaction with oxygen/protons species and stabilizes the catalytic active components during the OER process (Zhang, C.-L. et al., 2020).

CONCLUSION

To sum up, we reported a novel and efficient catalyst composed of hierarchically ultra-thin Co nanosheet arrays coupled with N-doped carbon plate through a feasible and easily scalable NaCl template method for a highly-efficient catalytic OER process. NaCl hard-template could provide a stable 2D platform for the formation and growth of self-assembled Co nanosheet arrays and 2D carbon plates during the dissolution-recrystallization-carbonization process. Benefitting from the vertically aligned ultrathin Co nanosheet arrays and hierarchically porous architecture, the obtained Co-NS@NCP possesses sufficient exposed active sites, excellent structure stability, and multidimensional mass transfer channels. As expected, the Co-NS@NCP affording remarkable electrocatalytic performance for OER in alkaline medium with a low overpotential of only 278 mV at 10 mA cm^{-2}, a small Tafel slope, as well as robust electrocatalytic stability for the long-term electrolysis process. The present findings here may shed a feasible and promising perspective for the development of high-efficiency noble-metal-free electrocatalysts for OER and energy storage and conversion system.

EXPERIMENTAL SECTION

Reagents and Chemicals

Cobalt nitrate hexahydrate ($Co(NO_3)_2{\cdot}6H_2O$), L-histidine dihydrochloride ($C_6H_{10}ClN_3O_2$), and sodium chloride (NaCl) were furnished from Sinopharm Chemical Regent Co., Ltd. (Shanghai, China). Commercial Ruthenium oxide (RuO_2) was purchased from Alfa Aesar Co., Ltd. All reagents and chemicals were used without further purification.

Synthesis of the Co-NS@NCP Catalysts

In a typical synthesis, 2.5 mM of L-histidine dihydrochloride, 5 g of NaCl, and 1 mM of $Co(NO_3)_2{\cdot}6H_2O$ are dissolved in 10 mL of deionized water with continuous vigorously magnetic stirring for 30 min to form a clear pink solution. Then, the solution was transferred into an open bottle and heated at 80°C for 5 h in an oil bath. Subsequently, this mixture was dried overnight in a vacuum oven to remove superfluous moisture. After that, the sediment was calcined in a tube furnace at 700°C for 2 h with a heating rate of 5°C/min in the N_2 atmosphere. The obtained black product was named Co-NS@NCP-700 and washed with ethanol and deionized water several times. Finally, the as-prepared Co-NS@NCP-700 was dried in an oven at 60°C overnight. For comparison, catalysts obtained from the above method under different pyrolysis temperatures of 600, 650, and 750°C are named Co-NS@NCP-600, Co-NS@NCP-650, and Co-NS@NCP-750, respectively.

Characterization

The crystalline and phase of the products were determined by X-ray powder diffraction (XRD) on a Rigaku D/max-RC diffractometer with a Cu Kα radiation ($\lambda = 1.5406$ Å). The morphology and structure of the products were represented by scanning electron microscopy (SEM, Hitachi S5500), transmission electron microscopy (TEM, JEOL JEM-2100F, 200 kV), and high-resolution transmission electron microscopy (HRTEM, JEOL JEM-2100F, 200 kV). High-angle annular dark-field scanning transmission electron microscopy (HAADF-STEM) and elemental mapping images were conducted on an FEI Tecnai G2 F20 microscope, which is built as an accessory to the JEOL JEM-2100F. The surface composition of materials was identified by X-ray photoelectron spectroscopy (XPS) on a Thermo VG Scientific ESCALAB 250 spectrometer with an Al Kα light source. Thermogravimetric analysis (TGA) was carried out under air with a temperature ramp of 10°C min^{-1} using a Netzsch SSTA 449C thermogravimetric analyzer (Netzsch STA 449C).

Electrochemical Measurement

All electrochemical tests were performed by using a conventional three-electrode system on a CHI 760E electrochemical analyzer at 25°C. In the three-electrode system, a glassy carbon electrode (GCE, 3 mm in diameter) served as a working electrode, a saturated calomel electrode (SCE) served as a reference electrode while a carbon electrode served as an auxiliary electrode. The 5 mg/mL of catalyst ink was prepared by ultrasonic dispersion method into a well-proportioned suspension as a working electrode. The solvents for the catalyst ink are water and ethanol in a ratio of 3:1. The 10 μL catalyst ink was evenly dropped to the surface of polished GCE and dried at room temperature. After that, 3 μL of 5 wt.% Nafion solution was dropped on the surface of catalyst modified GCE. The OER tests were implemented in O_2-saturated 1.0 M KOH solution with Linear Sweep Voltammetry (LSV) at a scan rate of 5 mV s^{-1} at 25°C. The electrochemical double-layer capacitances (C_{dl}) were obtained through a series of CV tests (scan rate: 20 ∼ 100 mV s^{-1}) at the potential range of 1.02 – 1.12 V. In this work, all the potentials were converted to a reversible hydrogen electrode (RHE). The equation of potential conversion from SCE to RHE is described in Equation (1):

$$E_{RHE} = E_{SCE} + 0.0592pH + 0.242 \quad (1)$$

DATA AVAILABILITY STATEMENT

The original contributions presented in the study are included in the article/**Supplementary Material**, further inquiries can be directed to the corresponding authors.

AUTHOR CONTRIBUTIONS

YT and DS planned the all experiments and wrote the manuscript. YW, ML, QZ, QW, and XZ synthesized the samples and performed the electrochemical measurements. All authors have read and approved it.

FUNDING

The work was financially supported by National Natural Science Foundation of China (22072067, 21875112). The authors are grateful for the supports from National and Local Joint Engineering Research Center of Biomedical Functional Materials and a project sponsored by the Priority Academic Program Development of Jiangsu Higher Education Institutions.

SUPPLEMENTARY MATERIAL

The Supplementary Material for this article can be found online at: https://www.frontiersin.org/articles/10.3389/fnano.2021.659865/full#supplementary-material

REFERENCES

Chandrasekaran, S., Ma, D., Ge, Y., Deng, L., Bowen, C., Roscow, J., et al. (2020). Electronic structure engineering on two-dimensional (2D) electrocatalytic materials for oxygen reduction, oxygen evolution, and hydrogen evolution reactions. *Nano Energy* 77:105080. doi: 10.1016/j.nanoen.2020.105080

Chen, B., He, X., Yin, F., Wang, H., Liu, D.-J., Shi, R., et al. (2017). MO-Co@N-doped carbon (M=Zn or Co): vital roles of inactive zn and highly efficient activity toward oxygen reduction/evolution reactions for rechargeable Zn-air battery. *Adv. Funct. Mater*. 27:1700795. doi: 10.1002/adfm.201700795

Chen, J., Fan, C., Hu, X., Wang, C., Huang, Z., Fu, G., et al. (2019). Hierarchically porous Co/Co_xM_y (M = P, N) as an efficient Mott-Schottky electrocatalyst for oxygen evolution in rechargeable Zn-air batteries. *Small* 15:e1901518. doi: 10.1002/smll.201901518

Chen, Q., Ding, R., Liu, H., Zhou, L., Wang, Y., Zhang, Y., et al. (2020). Flexible active-site engineering of monometallic Co-layered double hydroxides for achieving high-performance bifunctional electrocatalyst toward oxygen evolution and H_2O_2 reduction. *ACS Appl. Mater. Interfaces* 12, 12919–12929. doi: 10.1021/acsami.0c01315

Chen, R., Hung, S. F., Zhou, D., Gao, J., Yang, C., Tao, H., et al. (2019). Layered structure causes bulk NiFe layered double hydroxide unstable in alkaline oxygen evolution reaction. *Adv. Mater.* 31:e1903909. doi: 10.1002/adma.201903909

Chen, Y., Li, Z., Zhu, Y., Sun, D., Liu, X., Xu, L., et al. (2019). Atomic Fe dispersed on N-doped carbon hollow nanospheres for high-efficiency electrocatalytic oxygen reduction. *Adv. Mater.* 31:e1806312. doi: 10.1002/adma.201806312

Cheng, W., Zhao, X., Su, H., Tang, F., Che, W., Zhang, H., et al. (2019). Lattice-strained metal–organic-framework arrays for bifunctional oxygen electrocatalysis. *Nat. Energy* 4, 115–122. doi: 10.1038/s41560-018-0308-8

Dionigi, F., Zeng, Z., Sinev, I., Merzdorf, T., Deshpande, S., Lopez, M. B., et al. (2020). *In-situ* structure and catalytic mechanism of NiFe and CoFe layered double hydroxides during oxygen evolution. *Nat. Commun*. 11:2522. doi: 10.1038/s41467-020-16237-1

Dong, D., Wu, Z., Wang, J., Fu, G., and Tang, Y. (2019). Recent progress in Co_9S_8-based materials for hydrogen and oxygen electrocatalysis. *J. Mater. Chem. A* 7, 16068–16088. doi: 10.1039/C9TA04972J

Fragal, V. H., Fragal, E. H., Zhang, T., Huang, X., Cellet, T. S. P., Pereira, G. M., et al. (2019). Deriving efficient porous heteroatom-doped carbon electrocatalysts for hydrazine oxidation from transition metal ions-coordinated casein. *Adv. Funct. Mater*. 29:1808486. doi: 10.1002/adfm.201808486

Fu, G., Cui, Z., Chen, Y., Li, Y., Tang, Y., and Goodenough, J. B. (2017b). Ni_3Fe-N doped carbon sheets as a bifunctional electrocatalyst for air cathodes. *Adv. Energy Mater.* 7:1601172. doi: 10.1002/aenm.201601172

Fu, G., Cui, Z., Chen, Y., Xu, L., Tang, Y., and Goodenough, J. B. (2017a). Hierarchically mesoporous nickel-iron nitride as a cost-efficient and highly durable electrocatalyst for Zn-air battery. *Nano Energy* 39, 77–85. doi: 10.1016/j.nanoen.2017.06.029

Fu, G., Liu, Y., Chen, Y., Tang, Y., Goodenough, J. B., and Lee, J. M. (2018c). Robust N-doped carbon aerogels strongly coupled with iron-cobalt particles as efficient bifunctional catalysts for rechargeable Zn-air batteries. *Nanoscale* 10, 19937–19944. doi: 10.1039/C8NR05812A

Fu, G., Tang, Y., and Lee, J.-M. (2018d). Recent advances in carbon-based bifunctional oxygen electrocatalysts for Zn–air batteries. *ChemElectroChem* 5, 1424–1434. doi: 10.1002/celc.201800373

Fu, G., Wang, J., Chen, Y., Liu, Y., Tang, Y., Goodenough, J. B., et al. (2018a). Exploring indium-based ternary thiospinel as conceivable high-potential air-cathode for rechargeable Zn-air batteries. *Adv. Energy Mater*. 8:1802263. doi: 10.1002/aenm.201802263

Fu, G., Yan, X., Chen, Y., Xu, L., Sun, D., Lee, J. M., et al. (2018b). Boosting bifunctional oxygen electrocatalysis with 3D graphene aerogel-supported Ni/MnO particles. *Adv. Mater*. 30:1704609. doi: 10.1002/adma.201704609

Hua, Y., Xu, Q., Hu, Y., Jiang, H., and Li, C. (2019). Interface-strengthened CoP nanosheet array with Co_2P nanoparticles as efficient electrocatalysts for overall water splitting. *J. Energy Chem.* 37, 1–6. doi: 10.1016/j.jechem.2018.11.010

Huan, Y., Shi, J., Zou, X., Gong, Y., Xie, C., Yang, Z., et al. (2019). Scalable production of two-dimensional metallic transition metal dichalcogenide nanosheet powders using NaCl templates toward electrocatalytic applications. *J. Am. Chem. Soc*. 141, 18694–18703. doi: 10.1021/jacs.9b06044

Huang, C., Zhang, B., Luo, Y., Xiao, D., Tang, K., Ruan, Q., et al. (2020). A hybrid Co NPs@CNT nanocomposite as highly efficient electrocatalyst for oxygen evolution reaction. *Appl. Surf. Sci*. 507:145155. doi: 10.1016/j.apsusc.2019.145155

Jin, W., Chen, J., Liu, B., Hu, J., Wu, Z., Cai, W., et al. (2019). Oxygen vacancy-rich in-doped CoO/CoP heterostructure as an effective air cathode for rechargeable Zn-air batteries. *Small* 15:e1904210. doi: 10.1002/smll.201904210

Jothi, V. R., Karuppasamy, K., Maiyalagan, T., Rajan, H., Jung, C. Y., and Yi, S. C. (2020). Corrosion and alloy engineering in rational design of high current density electrodes for efficient water splitting. *Adv. Energy Mater.* 10:1904020. doi: 10.1002/aenm.201904020

Kang, B. K., Im, S. Y., Lee, J., Kwag, S. H., Kwon, S. B., Tiruneh, S., et al. (2019). *In-situ* formation of MOF derived mesoporous Co_3N/amorphous N-doped carbon nanocubes as an efficient electrocatalytic oxygen evolution reaction. *Nano Res.* 12, 1605–1611. doi: 10.1007/s12274-019-2399-3

Li, M., Pan, X., Jiang, M., Zhang, Y., Tang, Y., and Fu, G. (2020). Interface engineering of oxygen-vacancy-rich CoP/CeO_2 heterostructure boosts oxygen evolution reaction. *Chem. Eng. J.* 395:125160. doi: 10.1016/j.cej.2020.125160

Li, S., Hao, X., Abudula, A., and Guan, G. (2019). Nanostructured Co-based bifunctional electrocatalysts for energy conversion and storage: current status and perspectives. *J. Mater. Chem. A* 7, 18674–18707. doi: 10.1039/C9TA04949E

Li, S., Sirisomboonchai, S., Yoshida, A., An, X., Hao, X., Abudula, A., et al. (2018). Bifunctional $CoNi/CoFe_2O_4$ /Ni foam electrodes for efficient overall water splitting at a high current density. *J. Mater. Chem. A* 6, 19221–19230. doi: 10.1039/C8TA08223E

Li, T., Hu, Y., Pan, X., Yin, J., Li, Y., Wang, Y., et al. (2020). N-carbon supported hierarchical $Ni/Ni_{0.2}Mo_{0.8}N$ nanosheets as high-efficiency oxygen evolution electrocatalysts. *Chem. Eng. J.* 392:124845. doi: 10.1016/j.cej.2020.124845

Li, T., Li, S., Liu, Q., Tian, Y., Zhang, Y., Fu, G., et al. (2019). Hollow Co_3O_4/CeO_2 heterostructures *in situ* embedded in n-doped carbon nanofibers enable outstanding oxygen evolution. *ACS Sustain. Chem. Eng.* 7, 17950–17957. doi: 10.1021/acssuschemeng.9b04699

Li, Y., Zhong, C., Liu, J., Zeng, X., Qu, S., Han, X., et al. (2018). Atomically thin mesoporous Co_3O_4 layers strongly coupled with N-rGO nanosheets as

high-performance bifunctional catalysts for 1D knittable zinc-air batteries. *Adv. Mater*. 30:1703657. doi: 10.1002/adma.201703657

Liu, X., Gong, M., Xiao, D., Deng, S., Liang, J., Zhao, T., et al. (2020). Turning waste into treasure: regulating the oxygen corrosion on Fe foam for efficient electrocatalysis. *Small* 16:2000663. doi: 10.1002/smll.202000663

Lyu, D., Du, Y., Huang, S., Mollamahale, B. Y., Zhang, X., Hasan, S. W., et al. (2019). Highly efficient multifunctional Co-N-C electrocatalysts with synergistic effects of Co-N moieties and Co metallic nanoparticles encapsulated in a N-doped carbon matrix for water-splitting and oxygen redox reactions. *ACS Appl. Mater. Interfaces* 11, 39809–39819. doi: 10.1021/acsami.9b11870

Mishra, I. K., Zhou, H., Sun, J., Qin, F., Dahal, K., Bao, J., et al. (2018). Hierarchical CoP/Ni_5P_4/CoP microsheet arrays as a robust pH-universal electrocatalyst for efficient hydrogen generation. *Energy Environ. Sci*. 11, 2246–2252. doi: 10.1039/C8EE01270A

Ouyang, T., Ye, Y. Q., Wu, C. Y., Xiao, K., and Liu, Z. Q. (2019). Heterostructures composed of N-doped carbon nanotubes encapsulating cobalt and beta-Mo_2C nanoparticles as bifunctional electrodes for water splitting. *Angew. Chem. Int. Ed. Engl*. 58, 4923–4928. doi: 10.1002/anie.201814262

Sun, H., Tian, C., Fan, G., Qi, J., Liu, Z., Yan, Z., et al. (2020a). Boosting activity on Co_4N porous nanosheet by coupling CeO_2 for efficient electrochemical overall water splitting at high current densities. *Adv. Funct. Mater*. 30:1910596. doi: 10.1002/adfm.201910596

Sun, H., Yan, Z., Liu, F., Xu, W., Cheng, F., and Chen, J. (2020b). Self-supported transition-metal-based electrocatalysts for hydrogen and oxygen evolution. *Adv. Mater*. 32:e1806326. doi: 10.1002/adma.201806326

Wang, H., Qiu, X., Peng, Z., Wang, W., Wang, J., Zhang, T., et al. (2020). Cobalt-gluconate-derived high-density cobalt sulfides nanocrystals encapsulated within nitrogen and sulfur dual-doped micro/mesoporous carbon spheres for efficient electrocatalysis of oxygen reduction. *J. Colloid Interface Sci*. 561, 829–837. doi: 10.1016/j.jcis.2019.11.065

Wang, H., Qiu, X., Wang, W., Jiang, L., and Liu, H. (2019). Iron sulfide nanoparticles embedded into a nitrogen and sulfur co-doped carbon sphere as a highly active oxygen reduction electrocatalyst. *Front Chem*. 7:855. doi: 10.3389/fchem.2019.00855

Wang, J., and Zeng, H. C. (2018). CoHPi nanoflakes for enhanced oxygen evolution reaction. *ACS Appl. Mater. Interfaces* 10, 6288–6298. doi: 10.1021/acsami.7b17257

Wang, S., Wang, Y., Zang, S. Q., and Lou, X. W. (2019). Hierarchical hollow heterostructures for photocatalytic CO_2 reduction and water splitting. *Small Methods* 4:1900586. doi: 10.1002/smtd.201900586

Wu, Z. P., Lu, X. F., Zang, S. Q., and Lou, X. W. (2020). Non-noble-metal-based electrocatalysts toward the oxygen evolution reaction. *Adv. Funct. Mater*. 30:1910274. doi: 10.1002/adfm.201910274

Xie, W., Song, Y., Li, S., Li, J., Yang, Y., Liu, W., et al. (2019). Single-atomic-co electrocatalysts with self-supported architecture toward oxygen-involved reaction. *Adv. Funct. Mater*. 29:1906477. doi: 10.1002/adfm.201906477

Xu, H., Shan, C., Wu, X., Sun, M., Huang, B., Tang, Y., et al. (2020). Fabrication of layered double hydroxide microcapsules mediated by cerium doping in metal–organic frameworks for boosting water splitting. *Energy Environ. Sci.* 13, 2949–2956. doi: 10.1039/D0EE02113J

Xu, N., Zhang, Y., Wang, M., Fan, X., Zhang, T., Peng, L., et al. (2019). High-performing rechargeable/flexible zinc-air batteries by coordinated hierarchical Bi-metallic electrocatalyst and heterostructure anion exchange membrane. *Nano Energy* 65:104021. doi: 10.1016/j.nanoen.2019.104021

Yang, C. C., Zai, S. F., Zhou, Y. T., Du, L., and Jiang, Q. (2019c). Fe_3C-Co nanoparticles encapsulated in a hierarchical structure of N-doped carbon as a multifunctional electrocatalyst for ORR, OER, and HER. *Adv. Funct. Mater*. 29:1901949. doi: 10.1002/adfm.201901949

Yang, L., Shi, L., Wang, D., Lv, Y., and Cao, D. (2018). Single-atom cobalt electrocatalysts for foldable solid-state Zn-air battery. *Nano Energy* 50, 691–698. doi: 10.1016/j.nanoen.2018.06.023

Yang, Y., Yao, H., Yu, Z., Islam, S. M., He, H., Yuan, M., et al. (2019a). Hierarchical nanoassembly of MoS_2/Co_9S_8/Ni_3S_2/Ni as a highly efficient electrocatalyst for overall water splitting in a wide pH range. *J. Am. Chem. Soc*. 141, 10417–10430. doi: 10.1021/jacs.9b04492

Yang, Y., Zeng, R., Xiong, Y., Disalvo, F. J., and Abruna, H. D. (2019b). Cobalt-based nitride-core oxide-shell oxygen reduction electrocatalysts. *J. Am. Chem. Soc*. 141, 19241–19245. doi: 10.1021/jacs.9b10809

Yin, J., Jin, J., Liu, H., Huang, B., Lu, M., Li, J., et al. (2020). $NiCo_2O_4$-based nanosheets with uniform 4 nm mesopores for excellent zn-air battery performance. *Adv. Mater.* 32:e2001651. doi: 10.1002/adma.202001651

Yu, L., Zhou, H., Sun, J., Qin, F., Luo, D., Xie, L., et al. (2017). Hierarchical Cu@CoFe layered double hydroxide core-shell nanoarchitectures as bifunctional electrocatalysts for efficient overall water splitting. *Nano Energy* 41, 327–336. doi: 10.1016/j.nanoen.2017.09.045

Yu, Y., Xiao, D., Ma, J., Chen, C., Li, K., Ma, J., et al. (2018). The self-template synthesis of highly efficient hollow structure Fe/N/C electrocatalysts with Fe–N coordination for the oxygen reduction reaction. *RSC Adv*. 8, 24509–24516. doi: 10.1039/C8RA03672A

Zang, W., Sumboja, A., Ma, Y., Zhang, H., Wu, Y., Wu, S., et al. (2018). Single Co atoms anchored in porous N-doped carbon for efficient zinc–air battery cathodes. *ACS Catal*. 8, 8961–8969. doi: 10.1021/acscatal.8b02556

Zhang, C.-L., Liu, J.-T., Li, H., Qin, L., Cao, F.-H., and Zhang, W. (2020). The controlled synthesis of Fe_3C/Co/N-doped hierarchically structured carbon nanotubes for enhanced electrocatalysis. *Appl. Catalysis B Environ.* 261:118224. doi: 10.1016/j.apcatb.2019.118224

Zhang, K., Xia, X., Deng, S., Xie, D., Lu, Y., Wang, Y., et al. (2019). N-doped CoO nanowire arrays as efficient electrocatalysts for oxygen evolution reaction. *J. Energy Chem.* 37, 13–17. doi: 10.1016/j.jechem.2018.11.013

Zhang, X., Zhang, S., Yang, Y., Wang, L., Mu, Z., Zhu, H., et al. (2020). A general method for transition metal single atoms anchored on honeycomb-like nitrogen-doped carbon nanosheets. *Adv. Mater.* 32:e1906905. doi: 10.1002/adma.201906905

Zhang, Y., Feng, L., Zhan, W., Li, S., Li, Y., Ren, X., et al. (2020). Co_3O_4 hollow porous nanospheres with oxygen vacancies for enhanced Li–O_2 batteries. *ACS Appl. Energy Mater.* 3, 4014–4022. doi: 10.1021/acsaem.0c00426

Zhao, S., Yang, J., Han, M., Wang, X., Lin, Y., Yang, R., et al. (2020). Synergistically enhanced oxygen reduction electrocatalysis by atomically dispersed and nanoscaled Co species in three-dimensional mesoporous Co, N-codoped carbon nanosheets network. *Appl. Catalysis B Environ.* 260:118207. doi: 10.1016/j.apcatb.2019.118207

Zhao, T., Gadipelli, S., He, G., Ward, M. J., Do, D., Zhang, P., et al. (2018). Tunable bifunctional activity of $Mn_xCo_{3-x}O_4$ nanocrystals decorated on carbon nanotubes for oxygen electrocatalysis. *ChemSusChem* 11, 1295–1304. doi: 10.1002/cssc.201800049

Zheng, X., Cao, X., Sun, Z., Zeng, K., Yan, J., Strasser, P., et al. (2020). Indiscrete metal/metal-N-C synergic active sites for efficient and durable oxygen electrocatalysis toward advanced Zn-air batteries. *Appl. Catalysis B Environ.* 272:118967. doi: 10.1016/j.apcatb.2020.118967

Zheng, Y., Jiao, Y., Zhu, Y., Cai, Q., Vasileff, A., Li, L. H., et al. (2017). Molecule-Level g-C_3N_4 coordinated transition metals as a new class of electrocatalysts for oxygen electrode reactions. *J. Am. Chem. Soc*. 139, 3336–3339. doi: 10.1021/jacs.6b13100

Zhou, G., Li, M., Li, Y., Dong, H., Sun, D., Liu, X., et al. (2019). Regulating the electronic structure of CoP nanosheets by o incorporation for high-efficiency electrochemical overall water splitting. *Adv. Funct. Mater*. 30:1905252. doi: 10.1002/adfm.201905252

Zhou, G., Ma, Y., Wu, X., Lin, Y., Pang, H., Zhang, M., et al. (2020). Electronic modulation by N incorporation boosts the electrocatalytic performance of urchin-like Ni_5P_4 hollow microspheres for hydrogen evolution. *Chem. Eng. J.* 402:126302. doi: 10.1016/j.cej.2020.126302

Zhou, J., Dou, Y., Zhou, A., Guo, R.-M., Zhao, M.-J., and Li, J.-R. (2017). MOF Template-directed fabrication of hierarchically structured electrocatalysts for efficient oxygen evolution reaction. *Adv. Energy Mater.* 7:1602643. doi: 10.1002/aenm.201602643

Zhu, L., Yang, P., Huan, Y., Pan, S., Zhang, Z., Cui, F., et al. (2020). Scalable salt-templated directed synthesis of high-quality MoS_2 nanosheets powders towards energetic and environmental applications. *Nano Res*. 13, 3098–3104. doi: 10.1007/s12274-020-2979-2

Zhu, X., Dai, J., Li, L., Wu, Z., and Chen, S. (2019). N,S-Codoped hierarchical porous carbon spheres embedded with cobalt nanoparticles as efficient bifunctional oxygen electrocatalysts for rechargeable zinc-air batteries. *Nanoscale* 11, 21302–21310. doi: 10.1039/C9NR07632H

Conflict of Interest: The authors declare that the research was conducted in the absence of any commercial or financial relationships that could be construed as a potential conflict of interest.

The handling Editor declared a past co-authorship with the authors QZ and YT.